Reaction-Diffusion Dynamics in a Microreactor - Theoretical Study

Igor PLAZL
Assoc. Prof., PhD Chem. Eng.
Chemical Engineering Division, Faculty of Chemistry and Chemical Technology, University of Ljubljana
Askerceva 5, SI-1000 Ljubljana, Slovenia

igor.plazl@fkkt.uni-lj.si

Mitja LAKNER
Ass. Prof., PhD Math.
Civil and Geodetic Faculty, University of Ljubljana
Jamova 2, SI-1000 Ljubljana, Slovenia

Abstract

In the last decade, Microreactor Technology (*MRT*) as a new concept in chemical engineering has demonstrated the advantages of microstructured devices for chemical reactions impressively. Microscale reactors are devices whose operations depend on precisely controlled design features with characteristic dimensions from submillimeter to submicrometer. Due to the small amount of chemicals needed and high rate of heat and mass transfer, the systems are especially suited for reactions with highly toxic, flammable, and explosive reactants.
The theoretical description of the reaction-diffusion process in a microreactor was investigated in this work. A two-dimensional mathematical model, containing convection, diffusion, and a second-order reaction terms, was developed to analyze and to forecast the reactor performance. Despite the small dimensions of microchannels, it is usually assumed that for liquid systems the transport of momentum is governed by the incompressible Navier-Stokes equations. A fully developed parabolic velocity profile in a microchannel was assumed and considered in proposed mathematical model. Using a wide range of theoretical operating conditions, expressed as different (*ReSc)* numbers *(0.01<ReSc<10),* a dimensionless concentration was calculated for the plug-flow reactor (*PFR*) model, the continuous stirred-tank reactor (*CSTR*) model, and microreactor 2D model. For the numerical solution of the model equations, an implicite finite-difference method improved by introduction of non-equidistant differences was used. All models were solved by *Mathematica 5.2*.

Introduction

Nano- and Microtechnology are currently areas of rapid growth with a huge field of applications. Microtechnology has uncovered new scientific solutions and challenges in a broad range of areas, from electronics, medical technology, and fuel production and processing to biotechnology, the chemical industry, environmental protection, and process safety. The microscale reactors are devices whose operations depend on precisely controlled design features with characteristic dimensions from submillimeter to submicrometer. Because of the small amounts of chemicals needed and the high rate of heat and mass transfer, microscale systems are especially suited for reactions with highly toxic, flammable, and explosive reactants [1,2]. The microscale reactors do not have to be scaled-up, but numbered-up. The fact is that Micro-reaction-technology (MRT) has demonstrated the advantages of microstructured devices for chemical reactions impressively. Numerous reactions, including many notable and industrially relevant reactions, have been tried out successfully in microreactors and more than 400 publications detailing these successes have appeared in peer-reviewed journals [3,4]. The small length scale of microreactors reduces transport limitations, giving nearly gradientless conditions desirable for the determination of reaction kinetics [5,6,7]. In the area of catalytic chemistry, microreactors are an extremely efficient tool for rapid catalyst screening and for combinatorial chemistry. In the past few years, several papers have discussed the field of miniaturization of catalytic reactors [8,9,10,11].

The goal of our study was to analyze and to forecast the behavior of a general second-order irreversible homogeneous reaction taking place in a continuous flow microreactor. A mathematical model was developed to describe and predict reactor performance at steady-state conditions. Microreactor simulations were compared with ideal plug-flow reactor (*PFR*) and continuous stirred-tank reactor (*CSTR*) models for a broad range of operating conditions. By application of *Mathematica* computational tool, an implicit finite-difference method was used to solve the system of 2D partial differential equations of a second order. A special attention was devoted to the non-equidistant differences in order to improve the stability and accuracy of the numerical solutions.

Mathematical model

Let us consider a second-order irreversible homogeneous reaction $A+bB \rightarrow cC$, taking place in the microchannel within the flow driven at parabolic velocity profile, developed in the y-direction. Reactive components A and B enter the channel in two parallel flows as is schematic presented on Figure 1.

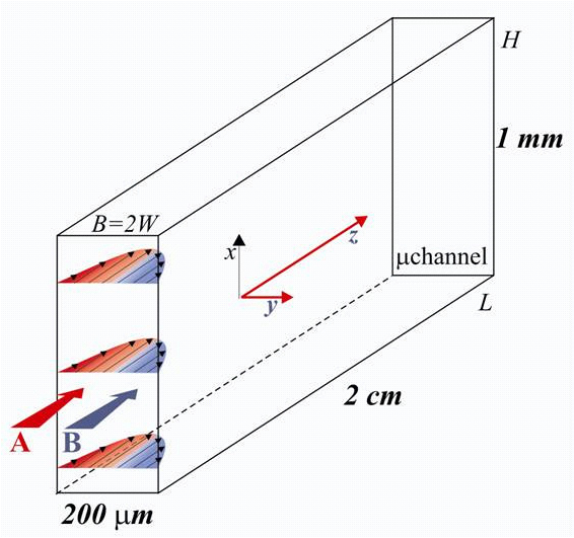

Figure 1. Microchannel scheme with dimensions used in simulations.

The reaction follows 2nd order kinetics $-r_A = k\, c_A\, c_B$, where k is the reaction rate constant ($m^3/mol\,s$). Microreactors are in general characterized by laminar flow observed for Re numbers up to 1000 [1]. Regarding operating conditions typical to microchannels, the laminar fluid flow in the z-axis direction is considered (Fig. 1). The velocity profile fully developed in the direction of the least dimension ($2W = 200\ \mu m$) can be therefore described as a function of y position only (Eq. 1)

$$v_z(y) = v_{max}\left[1-\left(\frac{y}{W}\right)^2\right] \tag{1}$$

For a general second-order irreversible homogeneous reaction in a microreactor with laminar fluid flow, a two-dimensional (2D) model is developed. The mass conservation equation, containing convection, diffusion, and a second-order reaction term for component A for control volume $H\Delta y\Delta z$ (Fig. 2) at steady-state conditions is

$$0 = v_z\,(H\,\Delta y)\,c_A\big|_z - v_z\,(H\,\Delta y)\,c_A\big|_{z+\Delta z} - D_{A,z}\,\frac{\partial c_A}{\partial z}\Big|_z\,(H\,\Delta y) + D_{A,z}\,\frac{\partial c_A}{\partial z}\Big|_{z+\Delta z}\,(H\,\Delta y) -$$

$$- D_{A,y}\,\frac{\partial c_A}{\partial y}\Big|_y\,(H\,\Delta z) + D_{A,y}\,\frac{\partial c_A}{\partial y}\Big|_{y+\Delta y}(H\,\Delta z) - k\,c_A\,c_B\,(H\,\Delta y\,\Delta z)$$

By rearrangement of all terms into the form required for taking the limits we get two-dimensional partial differential equation

$$v_{max}\left(1-\left(\frac{y}{W}\right)^2\right)\frac{\partial c_A}{\partial z} = D_A\left[\frac{\partial^2 c_A}{\partial z^2}+\frac{\partial^2 c_A}{\partial y^2}\right] - k c_A c_B \tag{2}$$

with associated boundary conditions

$$c_{A,0} = \begin{Bmatrix} c_{A,0} & 0 \le y \le W \\ 0 & -W \le y < 0 \end{Bmatrix}, \quad z = 0$$
$$\frac{\partial c_A}{\partial y}(z, \pm W) = 0 \tag{3}$$
$$\frac{\partial c_A}{\partial z}(L, y) = 0$$

After introduction of dimensionless concentrations and coordinates

$$X = \frac{c_A}{c_{A0}}, \quad Y = \frac{c_B}{c_{B0}}, \quad \psi = \frac{y}{W}, \quad \xi = \frac{z}{W}$$

we finally get the set of two-dimensionless partial differential equations with associated boundary condition in dimensionless form to analyze and to forecast the reactor performance at steady-state conditions for components A and B (Eqs. 4-7)

Reactant A

$$\left(1-\psi^2\right)\frac{\partial X}{\partial \xi} = \frac{1}{(Re\,Sc)_A}\left(\frac{\partial^2 X}{\partial \xi^2} + \frac{\partial^2 X}{\partial \psi^2}\right) - Da_A XY \tag{4}$$

b.c.

$$X(0,\psi) = \begin{cases} 1, & 1 \le \psi \le 0 \\ 0, & 0 < \psi \le -1 \end{cases}$$
$$\frac{\partial X(\xi, \pm 1)}{\partial \psi} = 0 \qquad 0 \le \xi \le \frac{L}{W}$$
$$\frac{\partial X\left(\frac{L}{W}, \psi\right)}{\partial \xi} = 0 \qquad 0 \le \psi \le 1 \tag{5}$$

Reactant B

$$\left(1-\psi^2\right)\frac{\partial Y}{\partial \xi} = \frac{1}{(Re\,Sc)_B}\left(\frac{\partial^2 Y}{\partial \xi^2} + \frac{\partial^2 Y}{\partial \psi^2}\right) - Da_B XY \tag{6}$$

b.c.

$$Y(0,\psi) = \begin{cases} 0, & 1 \le \psi \le 0 \\ 1, & 0 < \psi \le -1 \end{cases}$$
$$\frac{\partial Y(\xi, \pm 1)}{\partial \psi} = 0 \qquad 0 \le \xi \le \frac{L}{W}$$

$$\frac{\partial Y\left(\frac{L}{W},\psi\right)}{\partial \xi}=0 \qquad 0\le\psi\le 1 \tag{7}$$

In Equations 4 and 6 Da_A and Da_B are dimensionles Damköhler's numbers

$$Da_A=\frac{W\cdot c_{B0}k}{v_{max}} \quad Da_B=\frac{W\cdot c_{A0}k}{v_{max}} \tag{8}$$

and the inverse value of the product of Reynolds and Schmidt number is

$$\frac{1}{(Re\,Sc)}=\frac{1}{\frac{\rho v_{max}W}{\eta}\cdot\frac{\eta}{\rho D}}=\frac{D}{W\cdot v_{max}} \tag{9}$$

where are

v_{max} - maximal velocity (m/s), ρ - density (kg/m^3), η - dynamical viscosity ($Pa.s$), $c_{A,0}$ and $c_{B,0}$ - inlet concentrations of components A and B, respectively (mol/m^3), D - molecular diffusion coefficient (m^2/s), W - half width of the channel (m).

Numerical solutions

The finite differences were used to replace the partial derivates in the model equations (Eqs. 4-7). The discretization was done by the finite differences on a 2D Cartesian grid which in our case demands the implicit approach of solution.

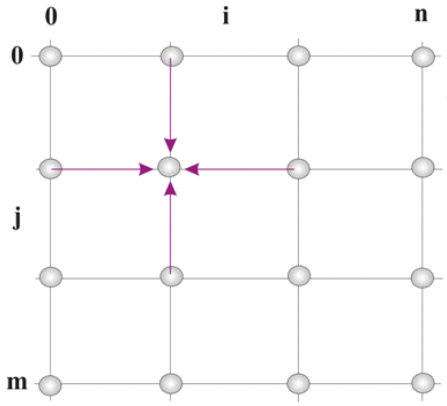

Figure 2. 2D Cartesian grid.

The replacement of the partial derivates resulting in the system of non-linear algebraic difference equations for the dependent variables at each grid point. The iterative algorithm is used to solve the system of non-linear algebraic equations for both components simultaneously. In the starting iteration procedure the known initial dimensionless concentration profile of component B i.e. $Y_{i,j}$ is used to solve the first approximation of the algebraic equation for component A i.e. $X_{i,j}$ (Eq. 10) and inversely.

$$X_{i,j}a'_{i,j} + X_{i+1,j}a''_j - bX_{i-1,j} - cX_{i,j+1} - cX_{i,j-1} = 0 \tag{10}$$

where

$$\left(1-\psi_j^{\,2}\right) = a_j \qquad \frac{1}{\Delta\xi\left(Re\,Sc\right)_A} = b \qquad Da_A\Delta\xi Y_{i,j} = d_{i,j} \qquad \frac{\Delta\xi}{\Delta\psi^2\left(Re\,Sc\right)_A} = c$$

$$-a_j + 2b + 2c + d_{i,j} = a'_{i,j} \qquad a_j - b = a''_j$$

with *i = 1,..., n-1 and j = 1,..., m-1*

The developed *Mathematica* code presented in Appendix enables the fast converging to the solution without fail. The Built-in *Mathematica* function *CoefficientArray* is used to build the matrix of the linear system. The stability and accuracy of the numerical solutions based on finite differences can be improved by introduction of non-equidistant differences. The comparison between classical equidistant and non-equidistant partition of grid points is schematically presented on Figures 3. and 4.

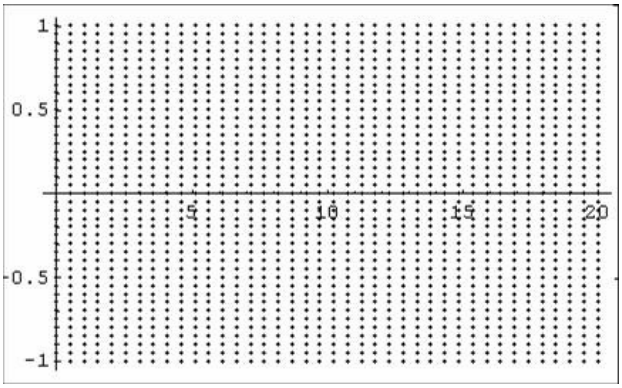

Figure 3. Classical equidistant partition of grid points.

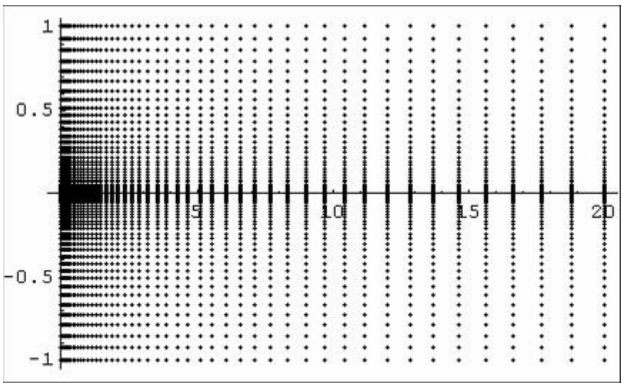

Figure 4. Non-equidistant partition of grid points.

Simple mathematical manipulation is needed to transform the equidistant finite differences (Eqs. 11., 12.)

$$f'(x_i) \approx \frac{y_{i+1} - y_{i-1}}{2h} \tag{11}$$

$$f''(x_i) \approx \frac{y_{i+1} - 2y_i + y_{i-1}}{h^2} \tag{12}$$

to the non-equidistant finite differences (Eqs. 13.,14.)

$$f'(x_i) \approx \frac{y_{i+1} - y_{i-1}}{h_{i-1} + h_i} \tag{13}$$

$$f''(x_i) \approx \left(\frac{y_{i+1} - y_i}{h_i} - \frac{y_i - y_{i-1}}{h_{i-1}} \right) \frac{2}{h_{i-1} + h_i} \tag{14}$$

Results and Discussion

Some characteristic concentration profiles of both components for selected operating conditions and process parameters (v_{av} = *0.001 m/s;* D_A = *1.1 10-9* m^2/s; D_B = *1.1 10-8* m^2/s; k = *0.9* $m^3/kmol\ s$) are presented on Figures 5 to 8 together with the dimensionless concentration profiles at the outlet of the microchannel. In the Figures 5 and 6 the dimensionless concentration profiles for component *A* and *B* respectively are presented in the case without chemical reaction (k = *0*) and only the dilution of components taking place in single-pass of flow through microchannel. The predicted outlet concentration profiles are in good agreement with the expected outlet concentration $c_{A,out}/c_{A,0}$ = *0.5.* The accuracy of the numerical solution is observable improved by introduction of non-equidistant differences (Fig. 6).

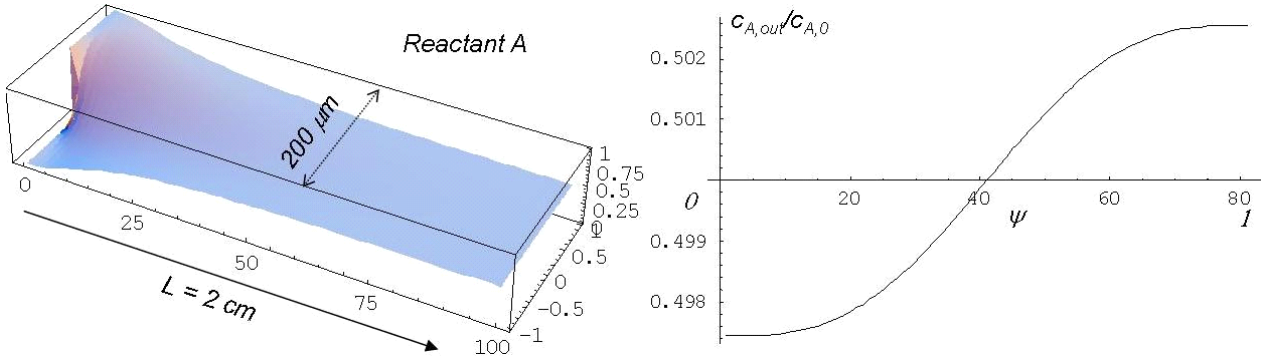

Figure 5. Steady-state dimensionless concentration profile in microchannel with the outlet profile of the component *A* without chemical reaction (equidistant differences).

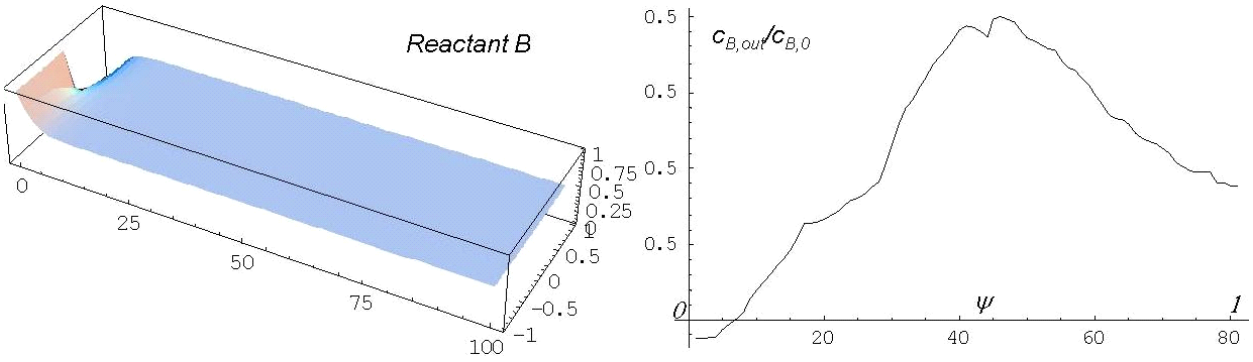

Figure 6. Steady-state dimensionless concentration profile in microchannel with the outlet profile of the component *B* without chemical reaction (non-equidistant differences).

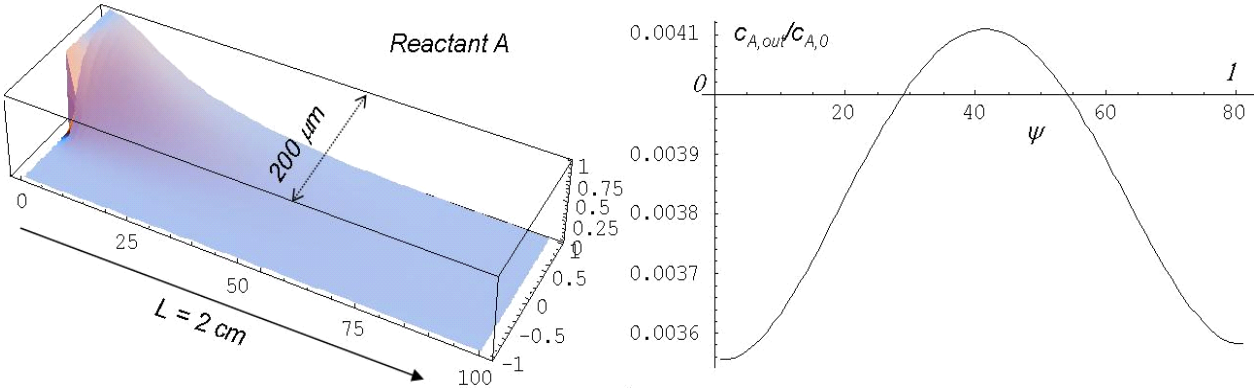

Figure 7. Steady-state dimensionless concentration profile in microchannel with the outlet profile of the reactant *A* (v_{av} = *0.001 m/s;* D_A = *1.1 10-9* m^2/s*;* D_B = *1.1 10-8* m^2/s*;* k = *0.9* $m^3/kmol\ s$).

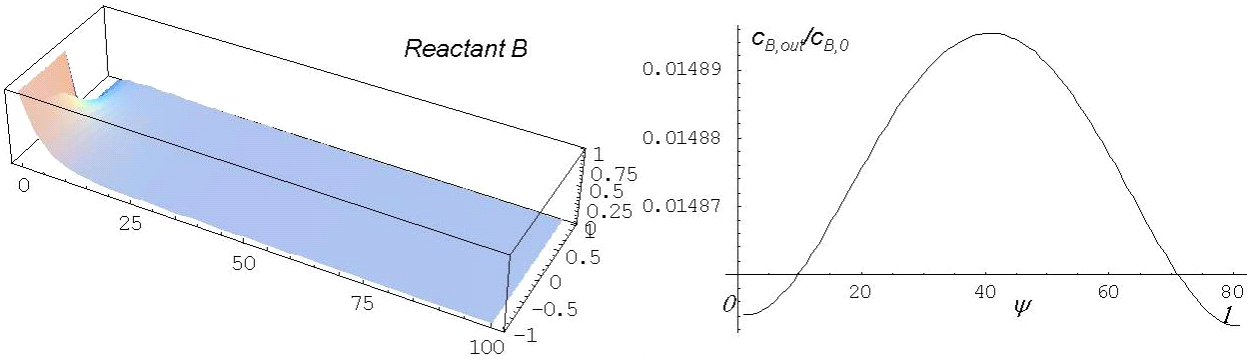

Figure 8. Steady-state dimensionless concentration profile in microchannel with the outlet profile of the reactant *B* (v_{av} = *0.001 m/s;* D_A = *1.1 10-9* m^2/s*;* D_B = *1.1 10-8* m^2/s*;* k = *0.9* $m^3/kmol\ s$).

In addition, the mass balance equations for the whole reactor in terms of relative concentration

($C_{A,out}/C_{A,0}$) of both plug-flow reactor (*PFR*) and ideal mixed-flow reactor (*CSTR*) (Figure 9) are required to compare the performance of different reactor types.

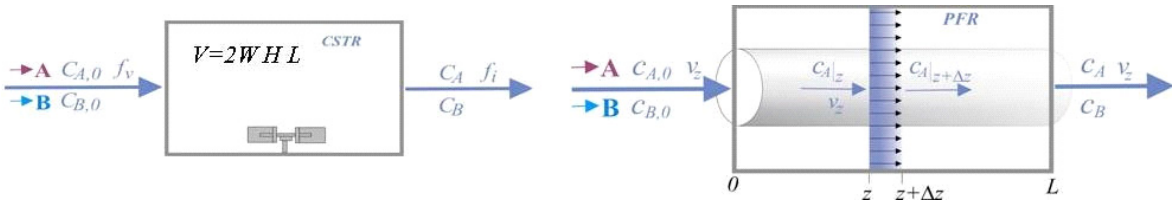

Figure 9. Schematic review of "microreactors" imitated the ideal behavior of *PFR* and *CSTR*.

Considering a second-order irreversible homogeneous reaction of the type $A+bB \rightarrow cC$, a dimensionless concentration of component *A* at steady-state conditions is given by

$$X_{PFR} = \frac{c_{A,out}}{c_{A,0}} = \frac{e^{DaM}(-1+M)X_0}{-e^{DaM}MX_0 + e^{Da}(-1+M-MX_0)} \tag{15}$$

for the plug-flow reactor, and

$$X_{CSTR} = \frac{c_{A,out}}{c_{A,0}} = \frac{-1+\sqrt{1+2Da+Da^2(-1+M)^2}+Da(-1+M)}{2DaM} \tag{16}$$

and for the ideal mixed-flow reactor. In cases when $M = b\ c_{A,0}/c_{B,0} = 1$, the upper equations (Eqs. 15, 16) are simplified to

$$X_{PFR} = \frac{1}{2+Da} \tag{17}$$

and

$$X_{CSTR} = \frac{-1+\sqrt{1+2Da}}{2Da} \tag{18}$$

respectively, where $D_A = k\ C_{B,0}\ L / v_{av}$.

Using a wide range of theoretical operating conditions ($0.01<Re{\cdot}Sc<10$), a dimensionless concentrations were calculated for the plug-flow reactor model, the continuous stirred-tank reactor model, and the microchannel 2D model and compared on Figure 10.

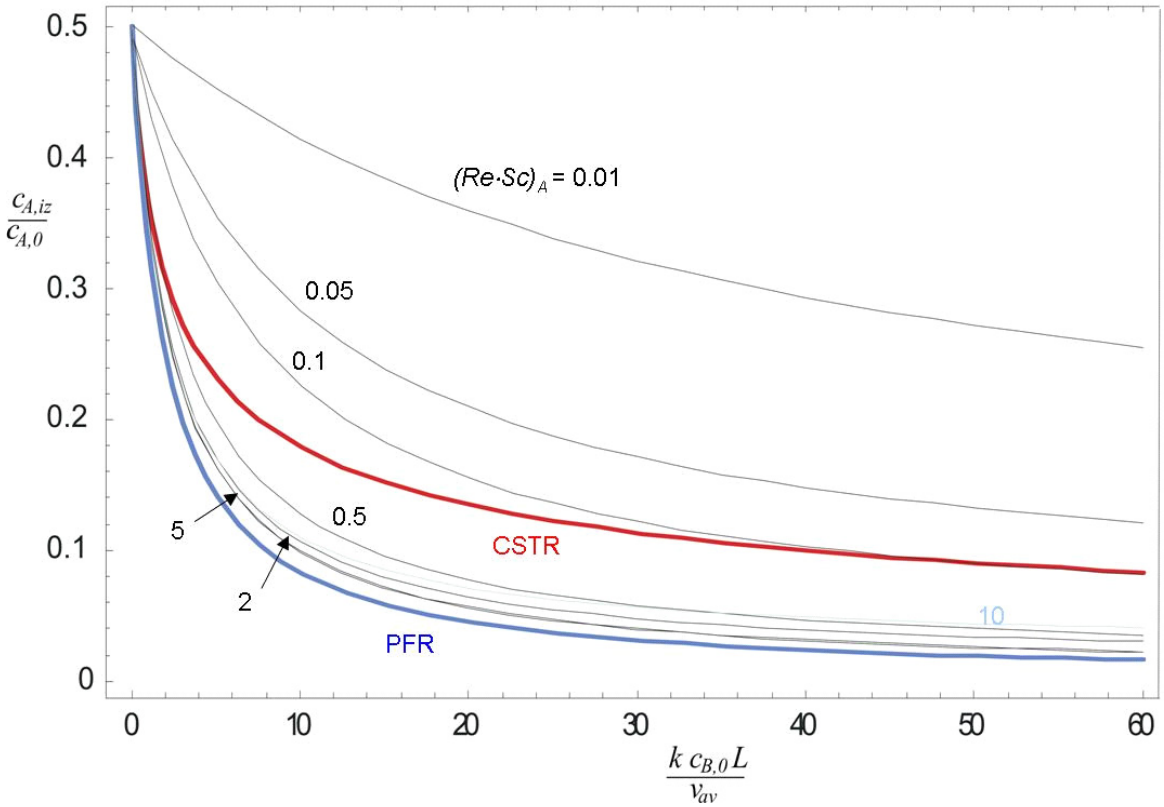

Figure 10. Comparison of the predictions of ideal *PFR* and *CSTR* models together with microchannel model simulations for a wide range of theoretical operating conditions, expressed as different *Re·Sc* numbers (*0.01<Re·Sc <10*).

Generally, an increase in the flow rate results in an increase in *Re·Sc*, and consequently, our model for the microreactor approaches that for a *PFR*. At *0.5<Re·Sc<10*, the model gives close-to-ideal PFR performance. As expected, a further increase in *Re·Sc* number (*Re·Sc>10*) results in the shifting away of the model simulations with the *PFR* curve. Namely, higher values of *Re·Sc* means higher velocities and smaller diffusion coefficients what is reflected in the shorter residence and reactions times. Only in the case of very low velocities, expressed as *Re·Sc* values below *0.1*, does the microreactor shift away from *CSTR* behavior (Figure 10). This phenomenon might be explained by the fact that at such small velocities and higher values of diffusion coefficients (*Re·Sc = 0.01 at v = 1 10^{-4} m/s and D = 6.610^{-7} m^2/s*) the diffusion of components in the flow direction (*z*-direction) become more significant.

Conclusions

The theoretical description of the reaction-diffusion process for a second-order irreversible homogeneous reaction in a microreactor was investigated. A developed mathematical model evaluated the microreactor performance. The microreactor model simulations were compared with ideal plug-flow reactor and continuous stirred-tank reactor models for a broad range of operating conditions in order to asses under what conditions (microchannel geometry, diffusion, convection, chemical kinetics) a given microreactor is more efficient/productive than classical macro-reactor. *Mathematica* code based on finite-difference method was developed to solve the

complex system of model equations. The numerical solutions were improved by introduction of non-equidistant differences. The presented mathematical model could be implicated for the different reaction types in homogeneous and non-homogeneous systems.

Acknowledgment

This work was supported through Grant P2-0191 Chemical Engineering, provided by the Ministry of Education, Science and Sport of the Republic of Slovenia.

Literature

[1] Jähnisch, K.; Hessel, V.; Löwe, H.; Baerns, M. Chemistry in microstructured reactors. *Angew. Chem., Int. Ed.* **2004**, 43, 406.

[2] Jensen, K. F. Microreaction engineerings: Is small better? *Chem. Eng. Sci.* **2001**, 56 (2), 293.

[3] Hessel, V., Lowe, H.; Organic synthesis with microstructured reactors. *Chem. Eng. Techn.* **2005**, 28 (3) 267-284.

[4] Watts, P., Haswell, S.J.; The application of microreactors for small scale organic synthe sis. Chem. Eng. Techn. 2005 28 (3), 290-301.

[5] Kuila, D.; Nagineni, V. S.; Potluri, A.; Zhao, S.; Aithal, R. K.; Liang, Y.; Fang, J.; Nassar, R.; Siriwardane, U.; Naidu, S. V.; Palmer, J. Microreactors for catalysis. *In Abstracts of Papers of the 226th ACS National Meeting; American Chemical Society*, Washington, DC, **2003**; Paper INOR-022.

[6] Ajmera, K. S.; Delattre, C.; Schmidt, A. M.; Jensen, K. F. Microreactors for measuring catalyst activity and determining reaction kinetics. *Stud. Surf. Sci. Catal.* **2003**, 145, 97.

[7] Roberge, D.M., Ducry, L., Bieler, N., Cretton, P., Zimmermann, B.; Microreactor technology: a revolution for the fine chemical and pharmaceutical industries? *Chem. Eng. Tech.* **2005**, 28 (3), 318-323.

[8] Wiessmeier G., Honicke, D.; Microfabricated components for heterogeneously catalyzed reactions. *J. Micromech. Microeng*. **1996**, 6, 285.

[9] Honicke, D. Microchemical reactors for heterogeneously catalyzed reactions. *Stud. Surf. Sci. Catal.* **1999**, 122, 47.

[10] Schouten, J. C., Rebrov, E. V., de Croon, M. H. J. M.; Miniaturization of heterogeneous catalytic reactor: Prospects for new developments in catalysis and process engineering. *Chimia* **2002**, 56, 627.

[11] Jovanovic, G.N., Žnidaršič Plazl, P., Sakrittichai, P., Al-Khaldi, K.; Dechlorination of p-Chlorophenol in a Microreactor with Bimetallic Pd/Fe Catalyst. *Ind. Eng. Chem. Res.* **2005**, 44, 5099-5106.

Appendix

The main part of the developed *Mathematica* code used in presented simulations of the described mathematical model

```
xy = Table[{(i/(n-1))^3.5 a, Sign[j] Abs[j/m]^3}, {i, 0, n - 1}, {j, -m, m}];
uA = uB = Table[0, {i, 0, n - 1}, {j, -m, m}];
h[i_, j_] := xy[[i + 1, j, 1]] - xy[[i, j, 1]];
k[i_, j_] := xy[[i, j + 1, 2]] - xy[[i, j, 2]];

var = Table[u[i, j], {i, 1, n}, {j, 1, 2 m + 1}] // Flatten;

equations[uAB_, z_, cAB_, KAB_] :=
 Join[Table[(1 - xy[[i, j, 2]]^2) (u[i+1,j]-u[i-1,j])/(h[i,j]+h[i-1,j]) ==
     cAB ((u[i,j+1]-u[i,j])/k[i,j] - (u[i,j]-u[i,j-1])/k[i,j-1]) 2/(k[i,j]+k[i,j-1]) - KAB uAB[[i, j]] u[i, j],
    {i, 2, n - 1}, {j, 2, 2 m}],
   Table[u[1, j] == z, {j, 1, m}], {u[1, m + 1] == 0.5}, Table[u[1, j] == 1 - z,
    {j, m + 2, 2 m + 1}], Table[u[n, j] == u[n - 1, j], {j, 2, 2 m}],
   Table[u[i, 1] == u[i, 2], {i, 2, n}],
   Table[u[i, 2 m + 1] == u[i, 2 m], {i, 2, n}]] // Flatten;

solve[uAB_, z_, cAB_, KAB_] := Module[{},
  {bb, A} = CoefficientArrays[equations[uAB, z, cAB, KAB], var];
  Partition[LinearSolve[A, -bb], 2 m + 1]];
step[{uA_, uB_}] := {solve[uB, 0, cA, KA], solve[uA, 1, cB, KB]};

uA1 = solve[uB, 0, cA, KA];
uB1 = solve[uA, 1, cB, KB];
{uAA, uBB} = NestWhile[step, {uA1, uB1}, (Max[Abs[#2 - #1]] > 10^-5) &, 2];
```